atmosphere

MDPI

Article

Analysis of Ionospheric VTEC Retrieved from Multi-Instrument Observations

Gurkan Oztan [1], Huseyin Duman [2], Salih Alcay [3,*], Sermet Ogutcu [3] and Behlul Numan Ozdemir [4]

[1] Department of Land Registry and Cadastre, Bor Vocational School, Nigde Omer Halisdemir University, Nigde 51700, Türkiye; oztangurkan@ohu.edu.tr
[2] Department of Geomatics Engineering, Engineering Faculty, Sivas Cumhuriyet University, Sivas 58140, Türkiye; hduman@cumhuriyet.edu.tr
[3] Department of Geomatics Engineering, Engineering Faculty, Necmettin Erbakan University, Konya 42090, Türkiye; sermetogutcu@erbakan.edu.tr
[4] Department of Geomatics Engineering, Faculty of Engineering and Natural Science, Konya Technical University, Konya 42250, Türkiye; bnozdemir@ktun.edu.tr
* Correspondence: salcay@erbakan.edu.tr

Abstract: This study examines the Vertical Total Electron Content (VTEC) estimation performance of multi-instruments on a global scale during different ionospheric conditions. For this purpose, GNSS-based VTEC data from Global Ionosphere Maps (GIMs), COSMIC (F7/C2)—Feng–Yun 3C (FY3C) radio occultation (RO) VTEC, SWARM–VTEC, and JASON–VTEC were utilized. VTEC assessments were conducted on three distinct days: geomagnetic active (17 March 2015), solar active (22 December 2021), and quiet (11 December 2021). The VTEC values of COSMIC/FY3C RO, SWARM, and JASON were compared with data retrieved from GIMs. According to the results, COSMIC RO–VTEC is more consistent with GIM–VTEC on a quiet day (the mean of the differences is 4.38 TECU), while the mean of FY3C RO–GIM differences is 7.33 TECU on a geomagnetic active day. The range of VTEC differences between JASON and GIM is relatively smaller on a quiet day, and the mean of differences on active/quiet days is less than 6 TECU. Besides the daily comparison, long-term results (1 January–31 December 2015) were also analyzed by considering active and quiet periods. Results show that Root Mean Square Error (RMSE) values of COSMIC RO, FY3C RO, SWARM, and JASON are 5.02 TECU, 6.81 TECU, 16.25 TECU, and 5.53 TECU for the quiet period, and 5.21 TECU, 7.07 TECU, 17.48 TECU, and 5.90 TECU for the active period, respectively. The accuracy of each data source was affected by solar/geomagnetic activities. The deviation of SWARM–VTEC is relatively greater. The main reason for the significant differences in SWARM–GIM results is the atmospheric measurement range of SWARM satellites (460 km–20,200 km (SWARM A, C) and 520 km–20,200 km (SWARM B), which do not contain a significant part of the ionosphere in terms of VTEC estimation.

Keywords: COSMIC RO; Feng–Yun 3C RO; GIM; JASON; SWARM; VTEC

check for updates

Citation: Oztan, G.; Duman, H.; Alcay, S.; Ogutcu, S.; Ozdemir, B.N. Analysis of Ionospheric VTEC Retrieved from Multi-Instrument Observations. *Atmosphere* **2024**, *15*, 697. https://doi.org/10.3390/atmos15060697

Academic Editors: Emilia Correia, Jean-Pierre Raulin, Paulo Roberto Fagundes and José-Valentin Bageston

Received: 23 April 2024
Revised: 6 June 2024
Accepted: 7 June 2024
Published: 9 June 2024

Copyright: © 2024 by the authors. Licensee MDPI, Basel, Switzerland. This article is an open access article distributed under the terms and conditions of the Creative Commons Attribution (CC BY) license (https://creativecommons.org/licenses/by/4.0/).

1. Introduction

The ionosphere is the layer of the atmosphere consisting of electrically charged atoms and molecules caused by solar radiation that extends from about 60 km to 1100 km above the Earth's surface. The ionosphere undergoes dynamic fluctuations, experiencing both regular (diurnal, seasonal, 27-day, 11-year, etc.) and irregular changes. The irregular variations of the ionosphere are caused by many factors, such as solar activities [1], geomagnetic storms [2], traveling ionospheric disturbances (TIDs) [3], ionospheric scintillations [4], volcanoes [5], earthquakes [6], etc. Due to the variations in the ionosphere and the effect of the ionosphere on satellite signals, it should be monitored regularly. As a result of the monitoring studies, various models have been developed for several decades (International Reference Ionosphere (IRI) [7], Parameterized Ionospheric model (PIM) [8], Bent model [9], NeQuick model [10,11], Semi–Empirical Low Latitude Ionospheric Model (SLIM) [12], IRI

PLAS [13], and more. The most widely used and regularly updated empirical model is the IRI model. The most recent version of the model is IRI–2020. Besides the Vertical Total Electron Content (VTEC), it provides monthly averages of the electron density, electron/ion temperature, and ion composition. Details of this model are given in Alcay [14] and Bilitza et al. [15]. However, these models are suitable for quiet ionospheric conditions.

Many data sources can be used in monitoring the ionosphere (Ionosonde, SWARM, Formosat/COSMIC, TSX, JASON, GRACE, GNSS). In recent years, the Global Navigation Satellite System (GNSS) has become a valuable tool for ionosphere-based studies [16–19]. One of the most important ionospheric quantities is the VTEC, which is capable of indicating variations within the ionosphere. It can be obtained using dual-frequency measurements [20]. The slant Total Electron Content (STEC) is calculated along a ray path between the satellite and receiver and then converted into VTEC by a mapping function. The details of the VTEC calculation are given in Senturk and Cepni [21]. VTEC data can be obtained on a station-based, regional, and global scale. Global ionosphere maps (GIMs) are offered by various analysis centers and are usually provided in the IONosphere EXchange format (IONEX) [22]. These maps are widely used in the studies associated with the ionosphere. There are many studies on the examination of ionospheric parameters obtained using different data sources [20,23–32]. Xu et al. [27] examined the ionospheric parameters retrieved from FY3C/COSMIC RO and found that FY3C RO TEC and COSMIC RO TEC correlated with GIM TEC by 95% and 92%, respectively. Milanowska et al. [20] evaluated the performance of GIMs over the oceans with respect to altimeter VTECs during high/low solar activity and geomagnetic storm periods. Vardhan et al. [26] compared GPS–TEC, Ionosonde TEC, COSMIC RO TEC, and SWARM TEC over the Indian region, and according to the results, the validation of ground-space-based TEC with GPS TEC was significantly observed.

Given the multi-instruments employed for ionospheric VTEC estimation, it becomes crucial to assess the compatibility of VTEC data from these sources across varying ionospheric conditions and ascertain the extent of any disparities. For this purpose, VTEC values obtained from JASON, SWARM, GIM, COSMIC RO, and FY3C RO on a global scale were examined with a comparative approach in this study. This study is significant because it will provide an initial insight into whether incorporating all available data sources would be advantageous in generating GIMs for various ionospheric conditions.

2. Data Sources

2.1. GIM VTEC

Global ionosphere maps (GIMs) are widely used in ionosphere-based research and positioning applications. Several ionosphere-associated analysis centers (IAACs) provide final, rapid, or real-time GIMs using different techniques. Among these agencies, the International GNSS Service (IGS), the Center for Orbit Determination in Europe (CODE), the European Space Agency (ESA), the Jet Propulsion Laboratory (JPL), the Polytechnic University of Catalonia (UPC), Natural Resources Canada (NRCan), the Chinese Academy of Sciences (CAS), and Wuhan University (WHU) provide the final GIMs. CODE, ESA, JPL, UPC, CAS, and WHU also provide rapid GIMs. In addition, UPC, CAS, and the Centre National d'Etudes Spatiales (CNES) provide Real-Time (RT) GIMs. Details of GIMs, including the methods used, are given by Yang et al. [33]. In this study, the final GIMs of the CODE data center were used. The spatial resolution of CODE's final GIMs is 2.5° latitude and 5° longitude, and the time resolution is 1 h.

2.2. COSMIC and FY3C Radio Occultation Data

The FORMOSAT–3/COSMIC (F3/C) mission was started in 2006 with six Low-Earth-Orbit (LEO) satellites in different orbital planes with an inclination of 72 degrees at 800 km altitude; the FORMOSAT–7/COSMIC–2 (F7/C2) was launched on 25 June 2019 with the same number of LEO satellites into different orbital planes with 24 degree inclinations at 550 km altitude [24]. These missions are designed to provide atmospheric and ionospheric

RO soundings. COSMIC Data are provided by the COSMIC Data Analysis and Archive Center [34]. In order to derive electron density, the Abel inversion technique is used. COSMIC provides VTEC information in TEC0 (ionospheric content) and TEC1 (plasmaspheric content) terms. The addition of TEC0 to TEC1 provides reliable VTEC observation for an occulted location [26].

Feng–Yun 3C (FY3C) RO is the radio occultation project developed by the National Satellite Meteorological Center of China (NSMC). FY3C satellite was launched in 2013 with an orbital inclination of 98.75 degrees and an orbital altitude of about 836 km, which has Beidou and GPS occultation observation capabilities [27,35,36]. FY3C–RO observations are provided by NSMC [37]. In this study, VTEC data were obtained from FY3C RO by integrating electron density up to LEO altitude (Equation (1)), as the details are given in Xu et al. [27].

$$TEC = \int Neds \tag{1}$$

where Ne is the electron density and s denotes the height above the surface.

The VTEC values from FY3C RO include gross errors due to observation noise and ionospheric plasma inhomogeneity [32]. In this study, to remove unqualified products, the mean deviation (MD) method was applied as per the details given by Jiang et al. [32].

2.3. SWARM Data

The SWARM satellite mission of the European Space Agency is to survey Earth's magnetic and electric fields with high resolution using three Low Earth Orbit satellites, called Alpha (A), Bravo (B), and Charlie (C). SWARM satellites orbit the Earth at different altitudes. While SWARM A and C are orbited at around 460 km above the earth's surface (with an inclination of 87.35 degrees, separated by 1–1.5 of longitude), SWARM B flies at about 510–520 km altitude with an orbital inclination of 87.75 degrees [26,38]. These satellites are equipped with various instruments to measure several parameters such as strength, direction, and variation of Earth's magnetic field, electric field, plasma density, and TEC [39]. Ionospheric data from SWARM satellites can be downloaded through the retrieval interface of the virtual research service [40]. The details of the SWARM–VTEC estimation are provided in the document "Swarm level2 TEC product description" [41].

2.4. JASON 3 Data

The altimeter–derived VTEC data were initiated with the Topex/Poseidon satellites, followed by JASON–1, JASON–2, and finally JASON–3 satellites. JASON–3 is the last element of altimeter missions that provides data for sea/ocean regions since 12 February 2016 [28]. The JASON–3 satellite flies on the same ground track with a 254 pass, 10–day exact repeat cycle [42]. The orbital height of JASON–3 is 1336 km. JASON–3 can provide VTEC information up to this orbital altitude. Thus, VTEC information only includes the ionosphere layer and not the plasmaspheric part, above the orbital height. However, considering the VTEC data above and below this altitude in the atmosphere, it can be said that it contains a large part of it. JASON–VTEC is determined as follows:

$$VTEC = -\frac{dR \times f_{Ku}^2}{40.3} \tag{2}$$

where dR is the Ku band ionospheric range correction and f_{Ku}, is Ku band frequency (13.575 GHz). Some JASON–VTEC data may have gross errors due to the influence of measurement noise. In this study, to reduce the measurement noise, a 100 s median filter was applied to smooth the data. Smoothed JASON–VTEC values were used for comparison. Since JASON–3 data started in February 2016, while JASON–3 data were used for solar active and quiet days in 2021, JASON–2 data were used for active and quiet days in 2015. JASON 2/3 data were obtained from [43].

3. Space Weather Conditions and Indices

Events due to the sun or sources outside the solar system create a type of weather called space weather. A number of phenomena originate from space weather conditions that have an influence on Earth and the rest of the solar system (Solar flares, Solar wind, Solar radiation storms, Coronal mass ejections, Galactic cosmic rays, Solar EUV irradiance, etc.). For details on these phenomena, see Alcay and Gungor [44]. A geomagnetic storm is a major disturbance of Earth's magnetosphere caused by the solar wind. In this study, solar activity index (F10.7) and Geomagnetic storm indices (Kp, Dst) were taken into consideration [45]. For daily comparison, three different days were used: geomagnetic active (17 March 2015), solar active (22 December 2021), and quiet days (11 December 2021). In the long-term analysis, 123 geomagnetic/solar active days (kp $\geq$ 5, Dst ≤ -50, and F10.7 $\geq$ 140) and 242 quiet days were also taken into account.

4. Analysis of Daily Results

In order to examine the performance of different data sources on a daily basis, three different ionospheric conditions, geomagnetic active, solar active, and quiet days, were chosen. The reason for choosing these days is also to determine the influence of active and quiet days on the TEC estimation performance of each data source. When the indices are examined (Figure 1), it is seen that there is a severe storm in the post-noon hours on the geomagnetic active day (17 March 2015). On the solar active day, the F10.7 index is at 140 sfu (22 December 2021). There is no solar or geomagnetic activity on the quiet day (11 December 2021).

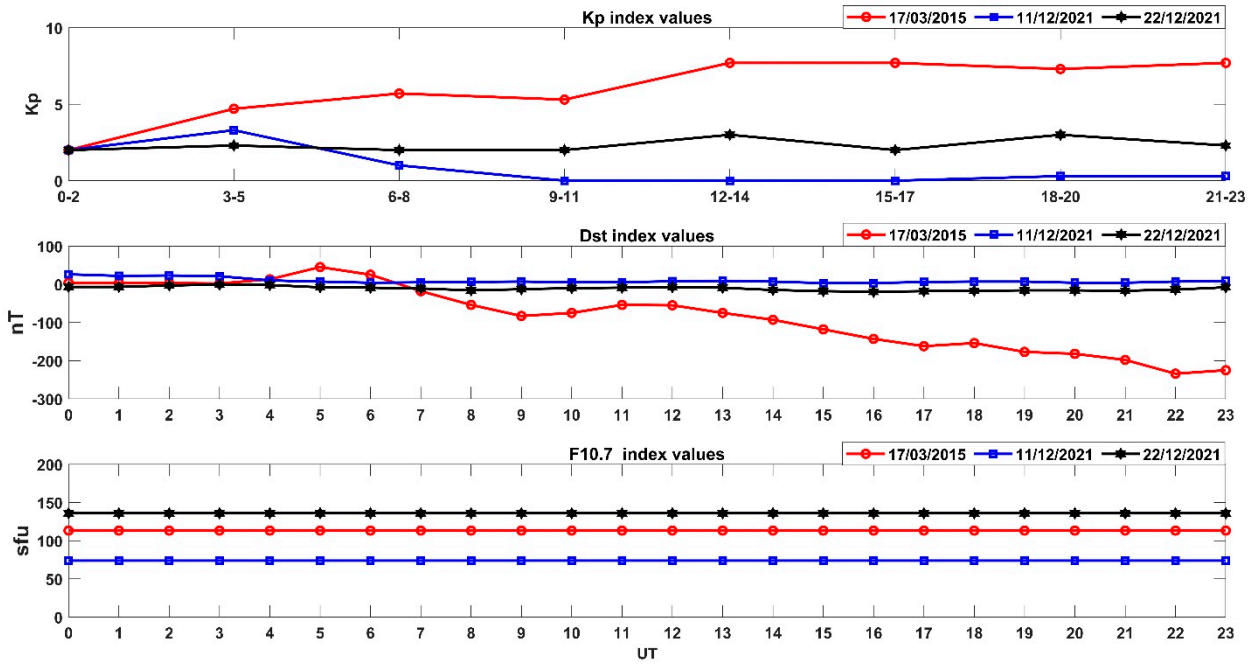


Figure 1. kp, dst, and F10.7 index values on geomagnetic active, solar active, and quiet days.

To ensure spatial and temporal harmony with the VTEC values obtained from COSMIC RO, FY3C RO, SWARM, and JASON at certain times, the corresponding GIM–VTEC values were obtained using bilinear interpolation. Comparative results of multi-instrument VTECs are given in the following subsections.

4.1. GIM VTEC versus COSMIC RO VTEC

In the analysis of COSMIC RO data, the data duration on active and quiet days was taken into account. For this purpose, five missions were used on the geomagnetic active day (17 March 2015) and one mission on the other two days. The occultation VTEC points

obtained from COSMIC RO missions, along with the GPS satellite number, are given in Figure 2. The Pseudo–Random Noise (PRN) numbers given in Figures 2–8 belong to the GPS satellites tracked by the Low Earth Orbit (LEO) satellites. Mission ID ranges from C001 to C006 and refers to six low–orbit satellites. In each mission, COSMIC RO TEC0, TEC1, and TEC0 + TEC1 values and corresponding GIM–VTEC values were calculated and given in Figures 3–8 for active and quiet days. Since TEC0 + TEC1 include ionosphere and plasmasphere, they are closer to the GIM–VTEC as expected. On the geomagnetic active day (17 March 2015), GIM or COSMIC RO underestimates/overestimates VTEC values, which differ according to the missions. For example, while PRN 24 mission ID C001 has higher GIM–VTEC values, PRN 30 mission ID C001 usually has larger COSMIC RO–VTEC values. On quiet (11 December 2021) and solar active (22 December 2021) days, the GIM TEC and COSMIC RO–VTEC values are quite compatible with each other, and the GIM–VTEC values are slightly higher.

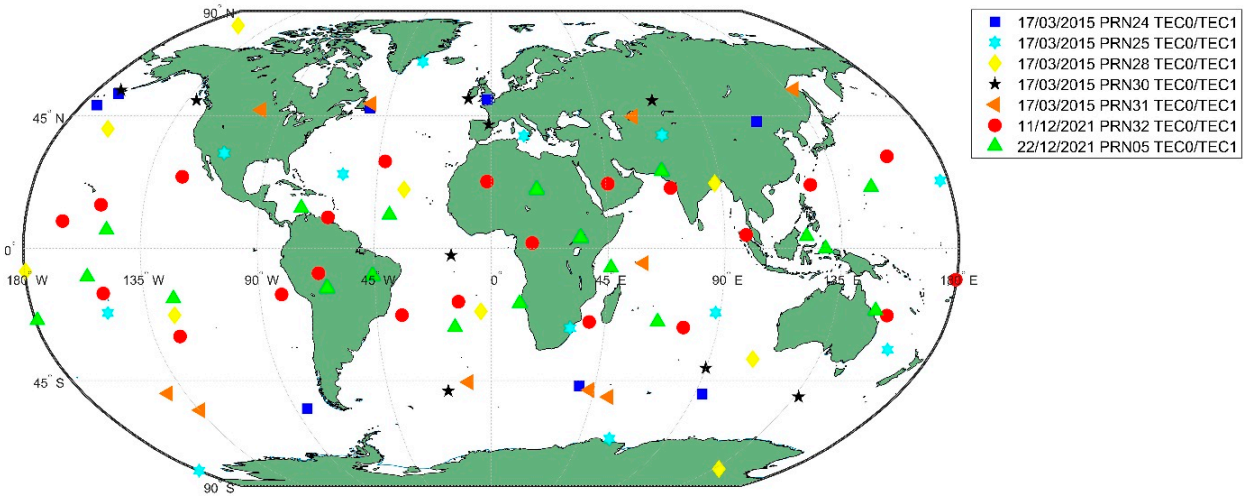


Figure 2. The used radio occultation VTEC points for active and quiet days.

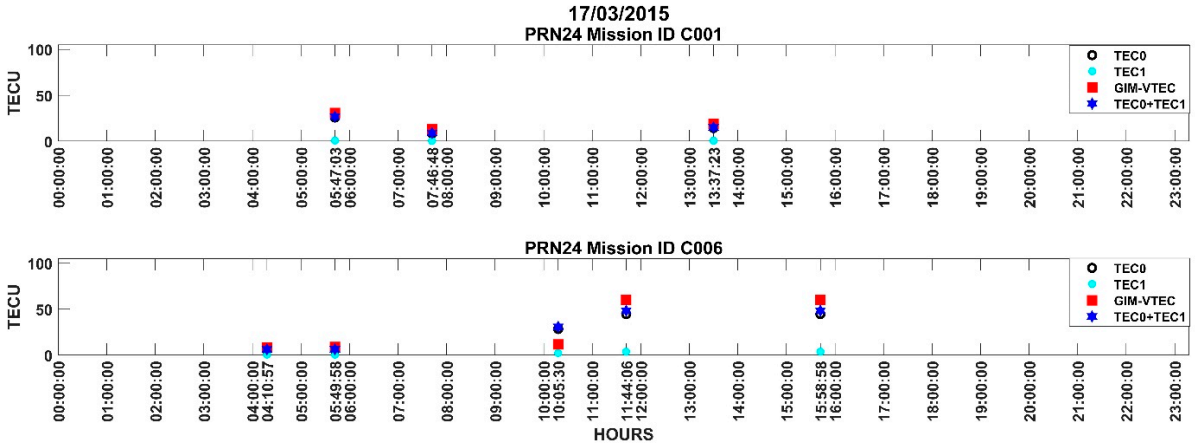


Figure 3. GIM–VTEC and Radio Occultation VTEC along with G24 Mission ID COO1/C006.

Besides the VTEC values obtained by the two methods, the basic statistical values, including maximum, minimum, mean, and Root Mean Square Error (RMSE) for GIM–VTEC and COSMIC RO–VTEC differences, were calculated and given in Table 1. To examine the accuracy of the VTEC from different data sources, RMS errors are used. The error (v) from COSMIC RO, FY3C RO, SWARM, and JASON to GIM is calculated using Equation (2)

$$v_i = TEC_i^G - TEC_i^{C/F/S/J} \quad (3)$$

where v_i is the absolute error between GIM and other measurements in the i-th pair, TEC_i^G denotes TEC derived from GIM, and $TEC_i^{C/F/S/J}$ represents COSMIC RO (C), FY3C RO (F), SWARM (S), and JASON (J) based TEC. The RMSE values are calculated as follows:

$$RMSE = \sqrt{\frac{1}{n}\sum_{i=1}^{n}(v_i)^2} \quad (4)$$

where n represents the number of data.

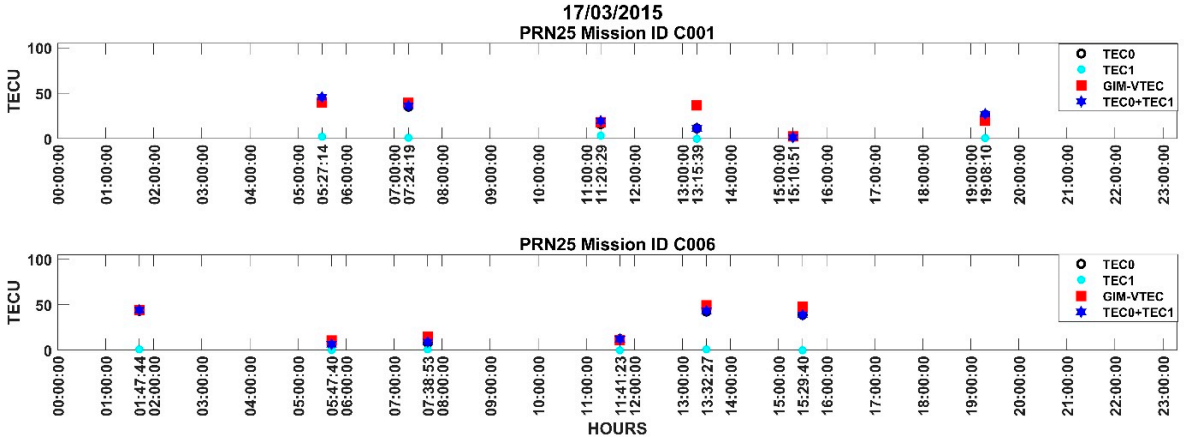


Figure 4. GIM–VTEC and Radio Occultation VTEC along with G25 Mission ID COO1/C006.

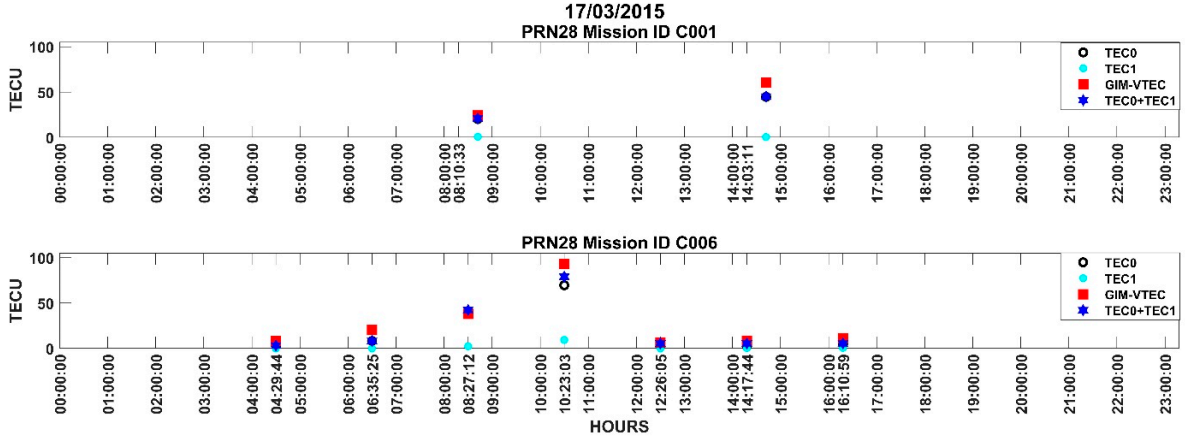


Figure 5. GIM–VTEC and Radio Occultation VTEC along with G28 Mission ID COO1/C006.

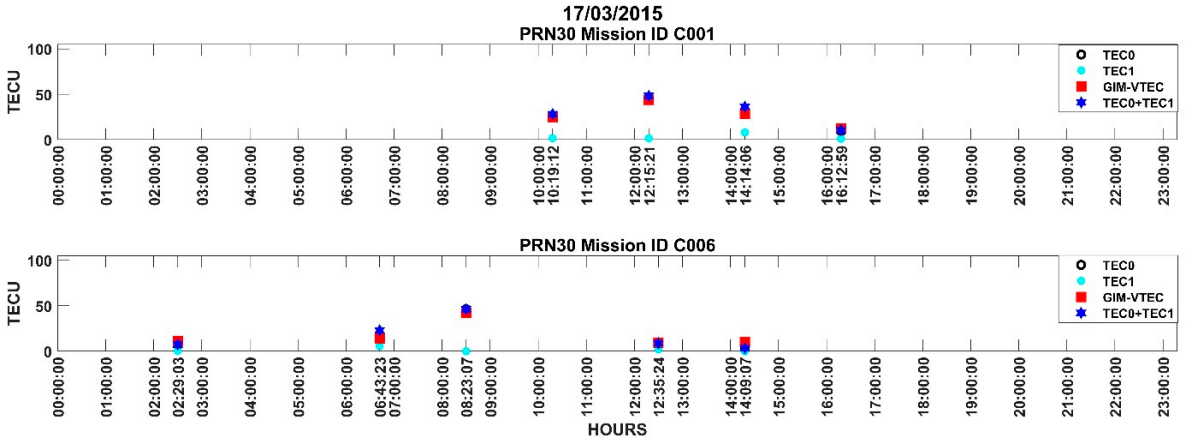


Figure 6. GIM–VTEC and Radio Occultation VTEC along with G30 Mission ID COO1/C006.

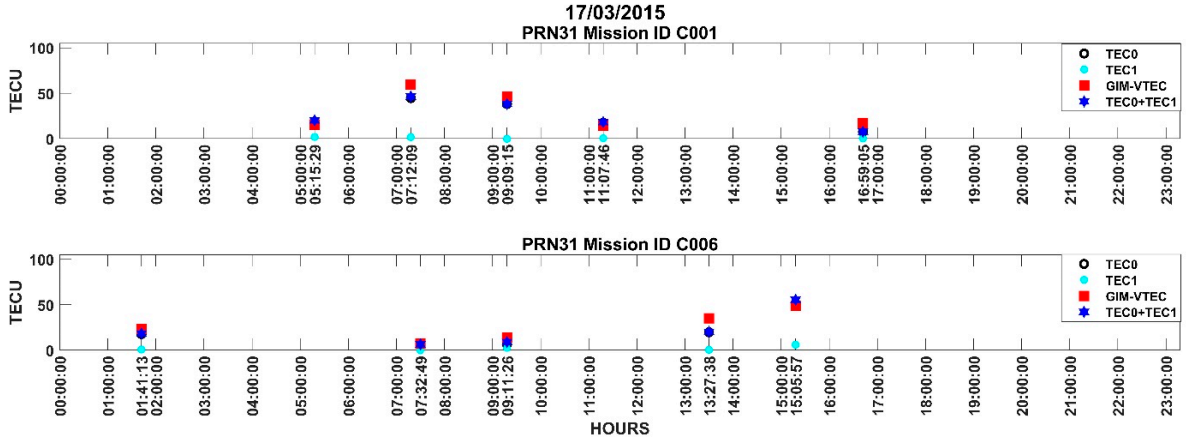


Figure 7. GIM–VTEC and Radio Occultation VTEC along with G31 Mission ID COO1/C006.

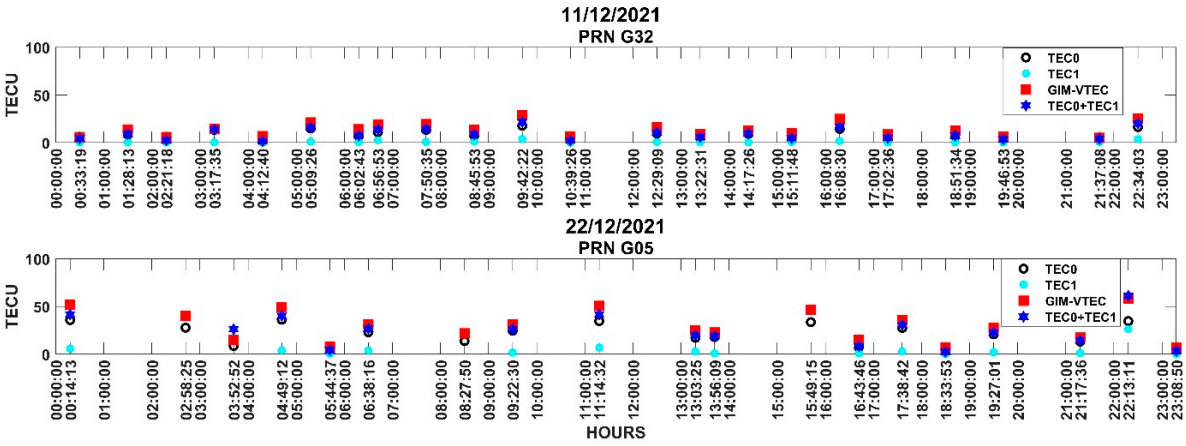


Figure 8. GIM–VTEC and Radio Occultation VTEC along with G32 and G05 for quiet (11 December 2021) and solar active day (22 December 2021) days.

Table 1. Basic statistical values of GIM–VTEC and COSMIC RO–VTEC differences for active and quiet days.

Date	Satellite	Maximum	Minimum	Mean	RMSE	VTEC Points
17 March 2015	24/25/28/30/31	19.14	0.20	6.21	7.66	48
11 December 2021	32	8.41	0.81	4.38	4.65	22
22 December 2021	05	11.45	2.82	5.78	6.35	19

In the table, VTEC points mean the number of data used within the scope of the paper for the relevant date. While five GPS satellites with the most data were selected on 17 March 2015, one satellite was selected for others. According to the table, the differences range between 0.20–19.14 TECU on the geomagnetic active day, 2.82–11.45 TECU on the solar active day, and 0.81–8.41 TECU on the quiet day. When the mean and RMSE values are examined, it is seen that the results obtained by the two methods on a quiet day are more compatible with each other than expected.

4.2. GIM VTEC versus FY3C RO VTEC

In order to evaluate the VTEC estimation performance of FY3C RO, only the geomagnetic active day was considered, as FY3C RO data were not available for quiet and solar active days. The occultation VTEC points obtained from FY3C RO missions, along with the GPS satellite numbers, are given in Figure 9. Figure 10 gives the VTEC values corresponding to GIM–VTEC and FY3C VTEC along the five missions with the highest data duration. The

differences range between 0.4 TECU and 26.02 TECU. The maximum, minimum, mean, and RMSE of the differences corresponding to 48 VTEC points are provided in Table 2. Although the differences are sometimes less than 1 TECU, the mean of the differences is 7.33 TECU.

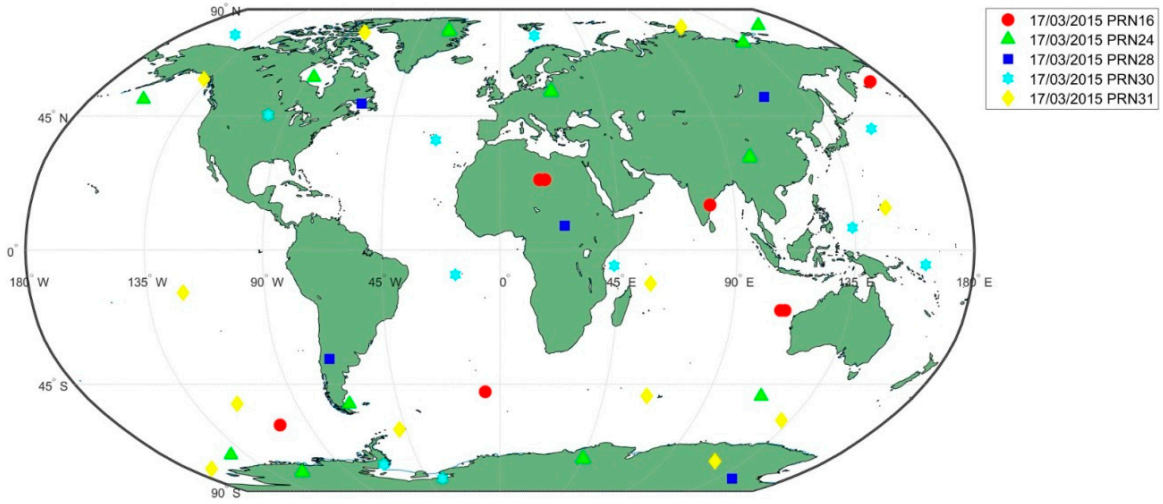


Figure 9. The used FY3C radio occultation VTEC points for active day.

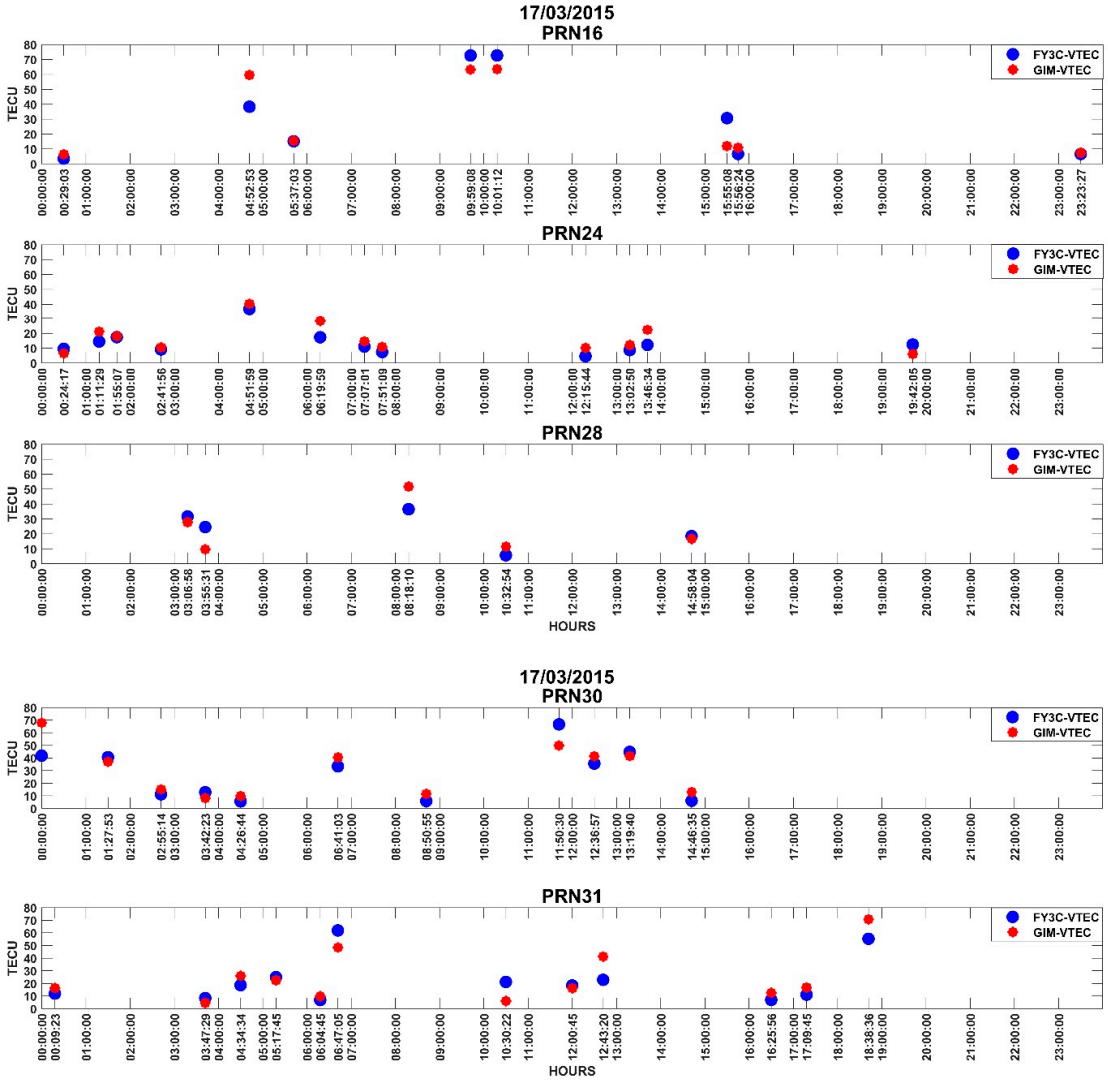


Figure 10. GIM–VTEC and FY3C RO–VTEC along with G16, G24, G28, G30, G31.

Table 2. Basic statistical values of GIM–VTEC and FY3C RO–VTEC differences for geomagnetic active day.

Date	Satellites	Maximum	Minimum	Mean	RMSE	VTEC Points
17 March 2015	16/24/28/30/31	26.02	0.40	7.33	9.42	48

4.3. GIM VTEC Versus SWARM VTEC

SWARM–VTEC data were obtained from SWARM–A, SWARM–B, and SWARM–C satellites at certain points in the world on geomagnetic/solar active and quiet days (Figure 11). SWARM–VTEC values and corresponding GIM–VTEC data are provided in Figures 12–14 for geomagnetic active, quiet, and solar active days, respectively. Upon examination of the VTEC values obtained through both methods, notable discrepancies are observed. The main reason for this is the vertical coverage of the SWARM satellites, which includes the region between the orbital heights of SWARM satellites and GPS satellite altitudes (462/511 km–20,200 km). When the basic statistical values of the differences are examined (Table 3), it is observed that the differences can exceed 34 TECU, although the differences are quite small in some periods. The mean of the differences is larger on active days than on quiet days.

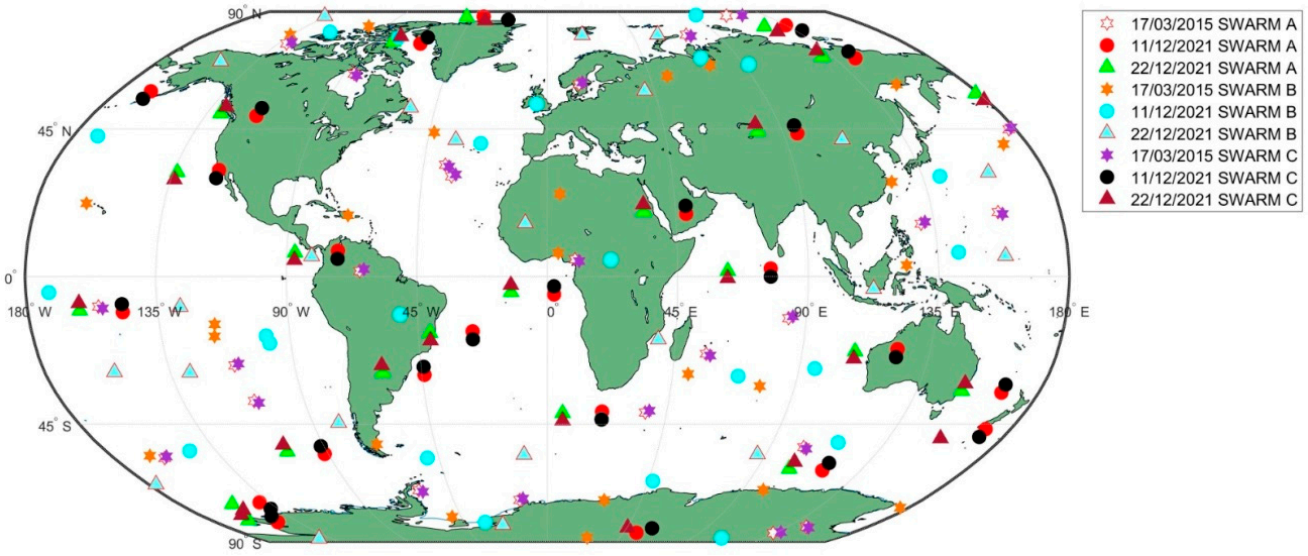


Figure 11. The used SWARM–VTEC points for active and quiet days.

Table 3. Basic statistical values of GIM–VTEC and SWARM–VTEC differences.

Date	Satellites	Maximum	Minimum	Mean	RMSE
17 March 2015	SWARM A	28.75	0.36	7.19	7.30
	SWARM B	32.50	3.48	13.15	9.66
	SWARM C	34.75	1.42	13.96	8.64
11 December 2021	SWARM A	25.75	0.25	7.23	7.26
	SWARM B	24.09	0.18	6.59	7.12
	SWARM C	25.71	0.14	7.11	6.99
22 December 2021	SWARM A	33.84	0.04	11.63	9.98
	SWARM B	34.79	0.45	13.15	10.73
	SWARM C	29.03	0.04	10.75	8.59

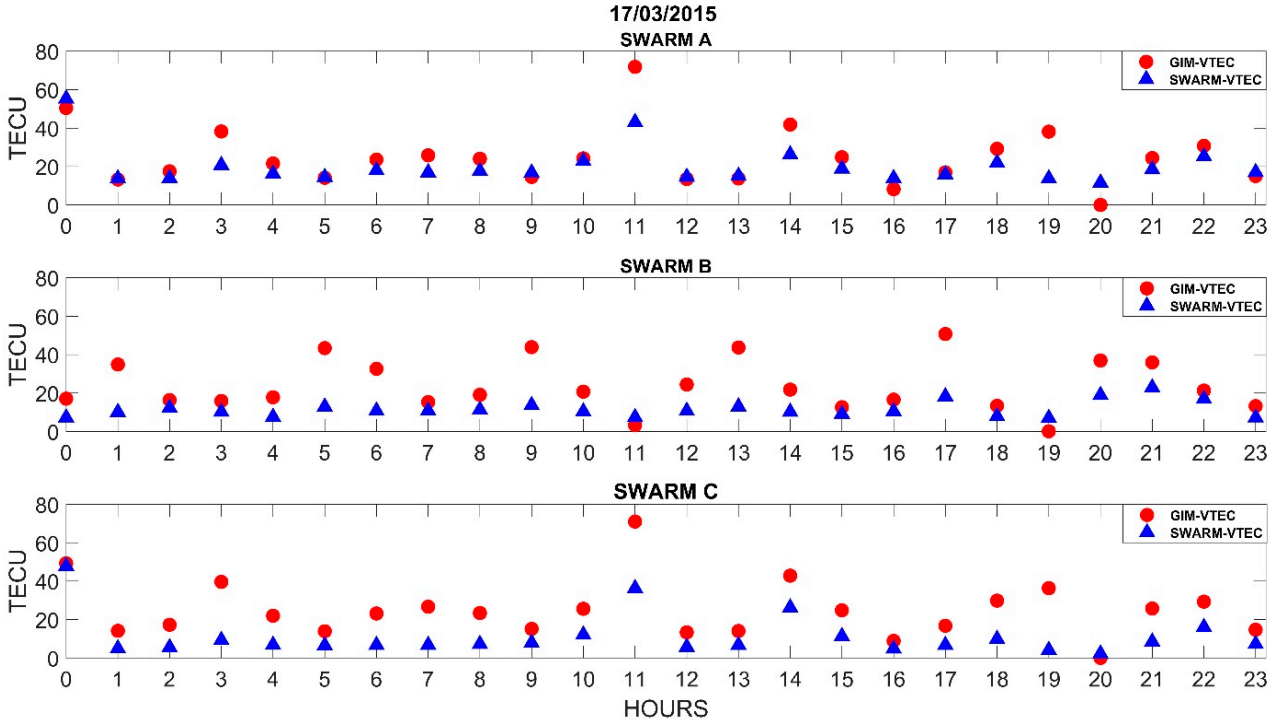


Figure 12. GIM–VTEC and SWARM–VTEC for geomagnetic active day along the GPS satellites.

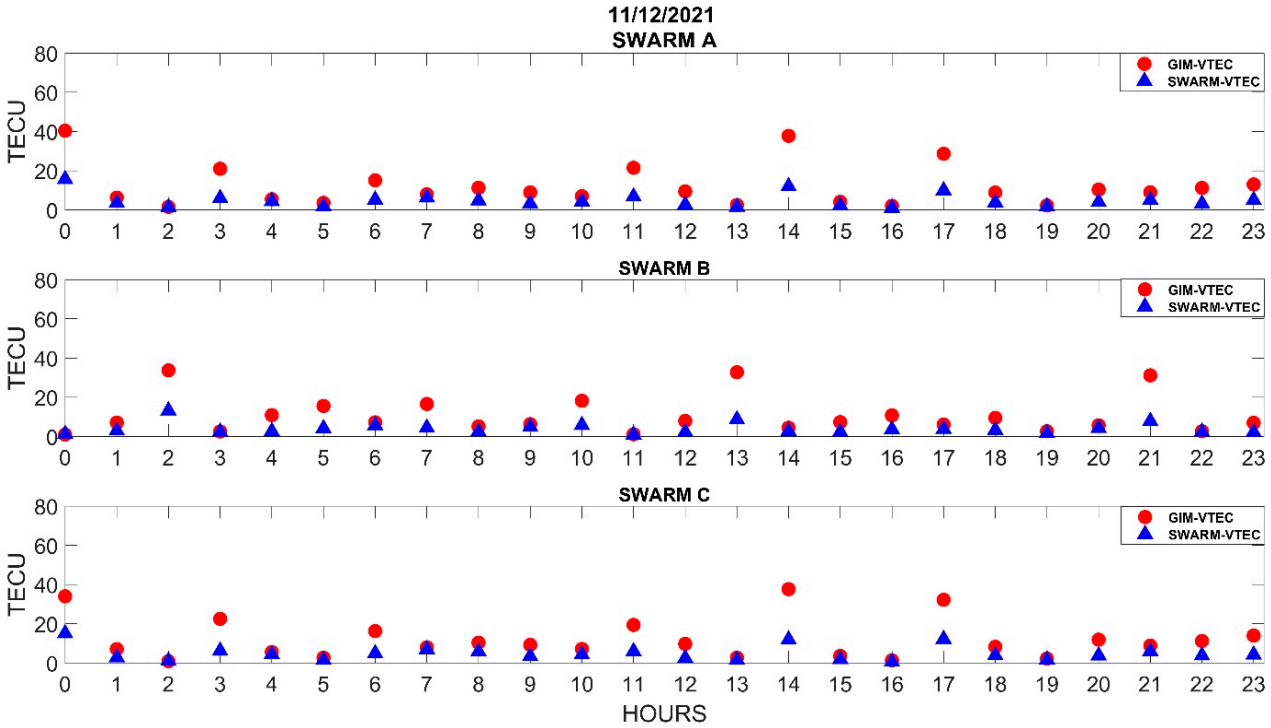


Figure 13. GIM–VTEC and SWARM–VTEC for quiet day along the GPS satellites.

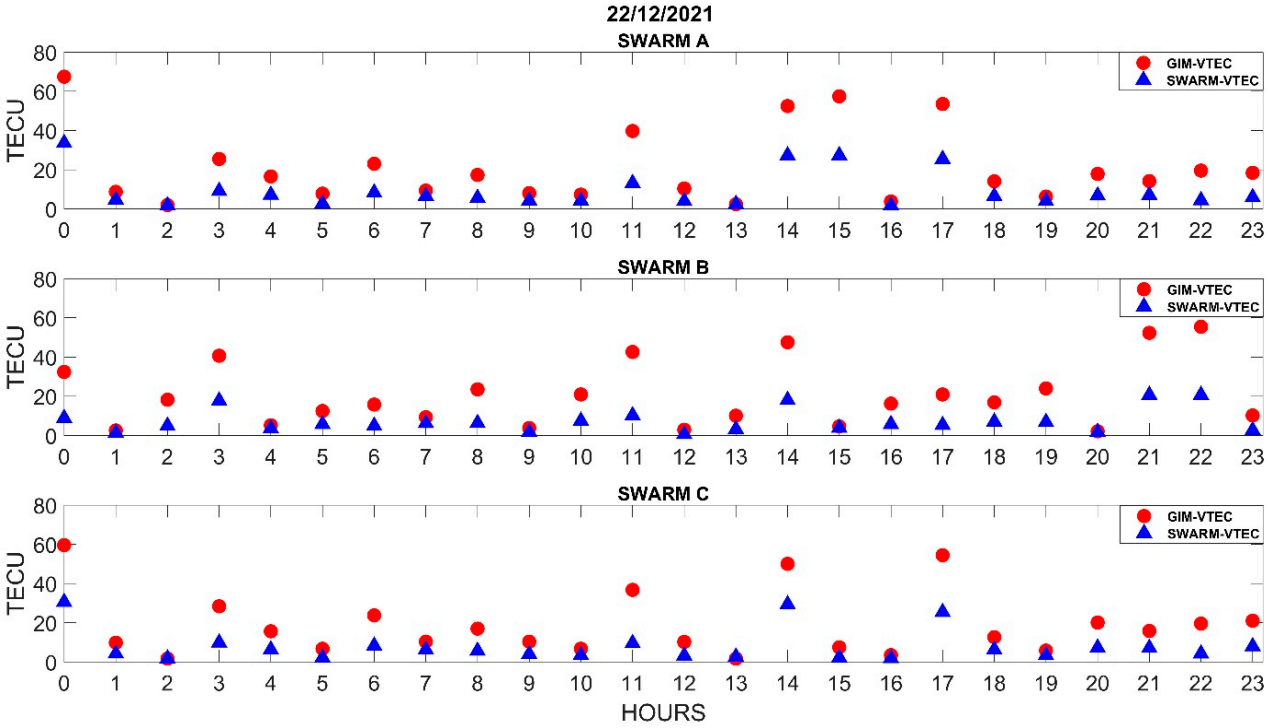


Figure 14. GIM–VTEC and SWARM–VTEC for solar active day along the GPS satellites.

4.4. GIM VTEC versus JASON VTEC

Since the JASON satellites only provide data over the ocean/sea, only these regions were considered in the comparison. The ground tracks of JASON–2 on geomagnetic active days and JASON–3 on solar active and quiet days are given in Figure 15. Details of the VTEC values obtained from the GIM at the same points as JASON on active and quiet days are given in Figure 16. JASON and GIM data are generally compatible with each other, particularly on the quiet day, and differences range between 1.41 and 10.92 TECU. When the mean/RMSE of the differences are examined, it is seen that 5.20/5.77 TECU on the quiet day, 5.75/7.88 TECU on the geomagnetic active day, and 4.93/5.80 TECU on the solar active day (Table 4).

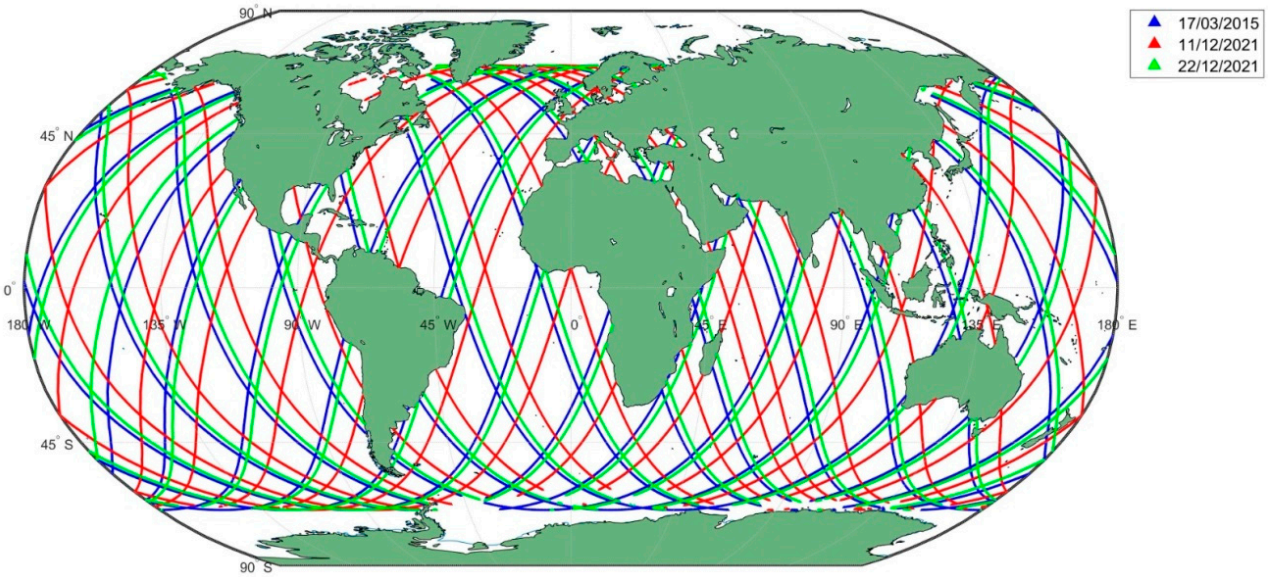


Figure 15. Daily ground track of JASON–2 on 17 March 2015 and JASON–3 on 11 December 2021 and 22 December 2021.

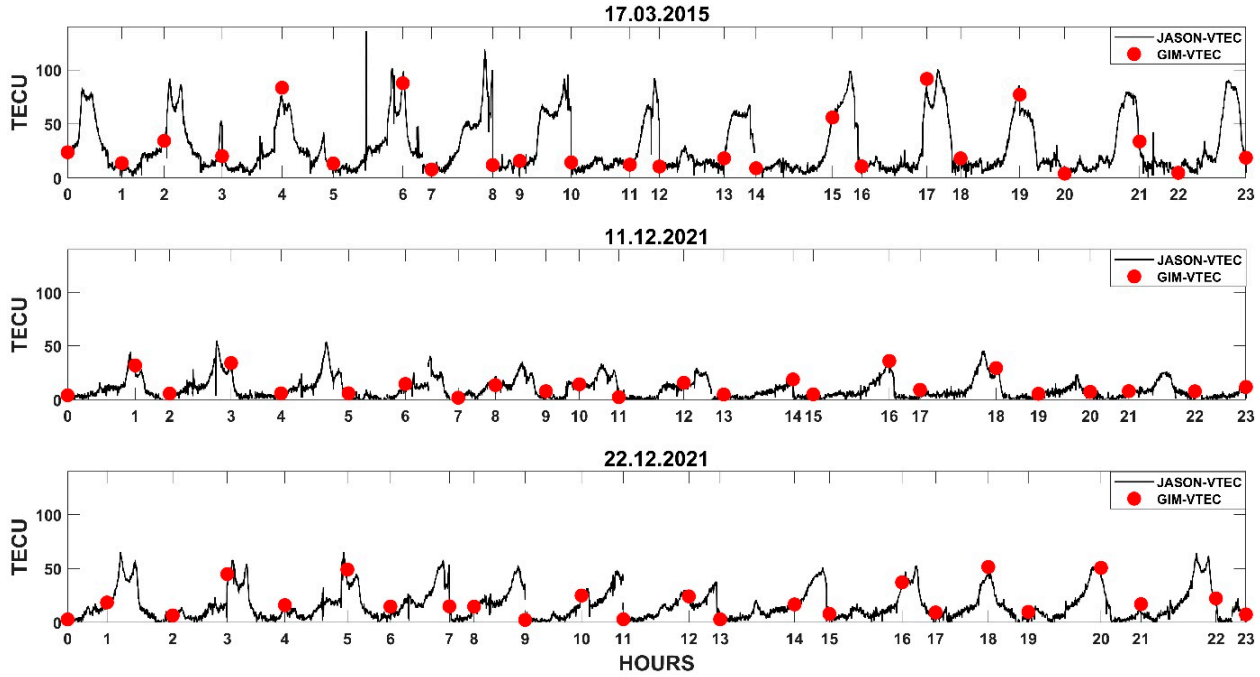


Figure 16. JASON–VTEC and GIM–VTEC values for active and quiet days.

Table 4. Basic statistical values of GIM–VTEC and JASON–VTEC differences.

Date	Maximum	Minimum	Mean	RMSE
17 March 2015	19.51	0.11	5.75	7.88
11 December 2021	10.92	1.41	5.20	5.77
22 December 2021	12.02	0.29	4.93	5.80

5. Analysis of Long-Term Results

Besides the daily results, to examine the long-term TEC estimation performance of various data sources with respect to GIM in 2015, 242 quiet days and 123 active days were chosen based on the criteria given in Section 3. Figures 17 and 18 show the linear fitting of COSMIC RO, FY3C, SWARM, and JASON–VTEC with respect to GIM–VTEC during quiet and active periods, respectively. The correlation coefficients of COSMIC RO, FY3C, SWARM, and JASON–VTEC with GIM–VTEC for the quiet period are 0.94, 0.89, 0.87, and 0.97, respectively (Figure 17). In Figure 17, it can be observed that point distributions between JASON–VTEC and GIM–VTEC are slightly more condensed around the fitting line compared to COSMIC, FY3C, and SWARM. Furthermore, the RMSE of COSMIC RO, FY3C RO, SWARM, and JASON are 5.02 TECU, 6.81 TECU, 16.25 TECU, and 5.53 TECU, respectively.

When the comparison results for active days are examined (Figure 18), it is seen that the correlation coefficient between JASON–VTEC and GIM–VTEC is 0.97, which is better than others. However, the distributions of points between JASON–VTEC and GIM–VTEC are mainly concentrated near the fitting line, while the distributions of the points between SWARM–VTEC and GIM–VTEC are more dispersed. The RMSE of data sources are slightly larger compared to the quiet period, which are 5.21 TECU, 7.07 TECU, 17.48 TECU and 5.90 TECU for COSMIC RO, FY3C RO, SWARM, and JASON, respectively. The results also show that the VTEC of SWARM exhibits a lower value consistent with that of GIM–VTEC for both active and quiet periods.

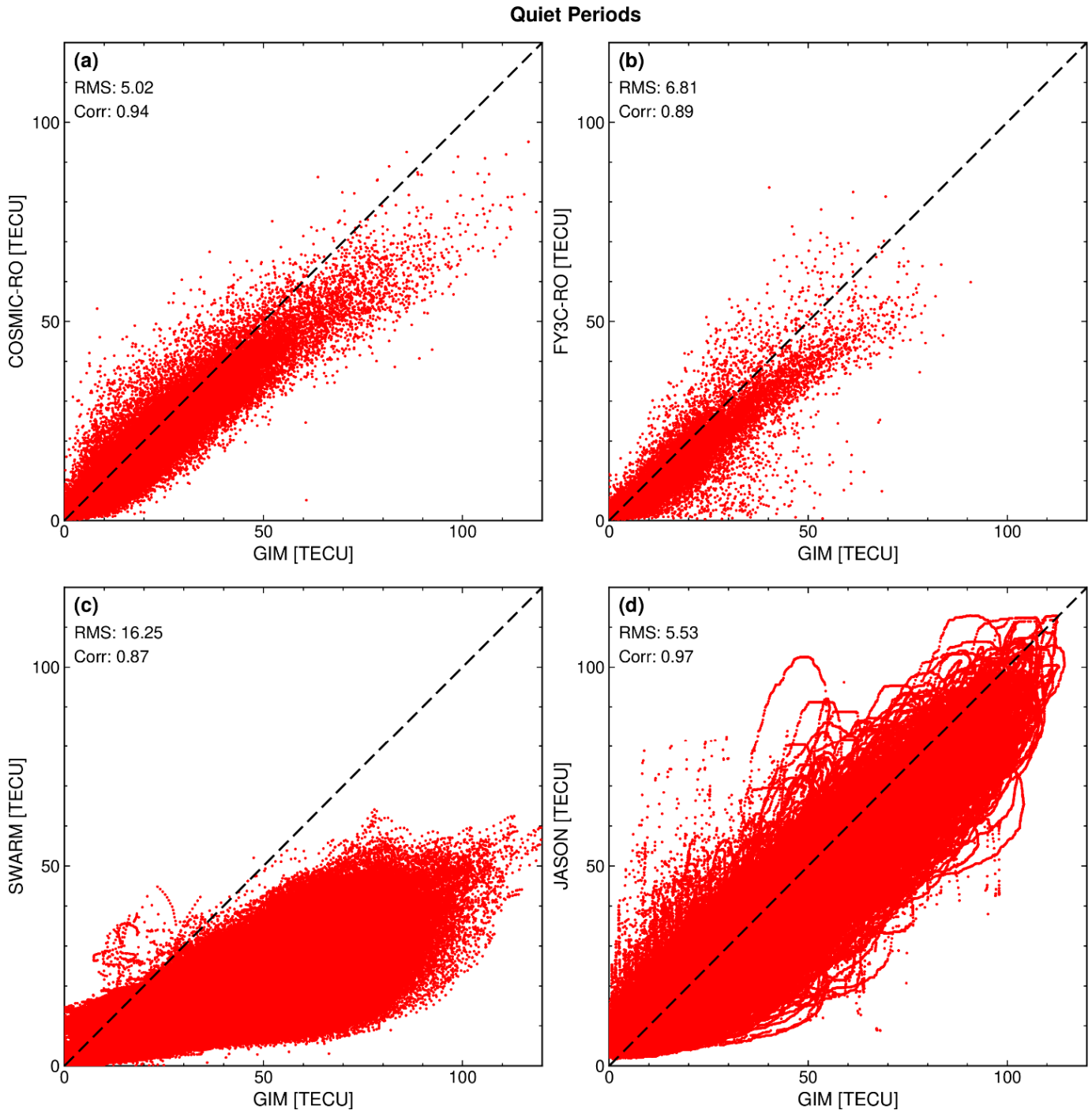


Figure 17. Scatter plots of VTEC values retrieved from COSMIC–RO (**a**), FY3C–RO (**b**), SWARM (**c**), and JASON (**d**) with GIM–VTEC for the quiet period.

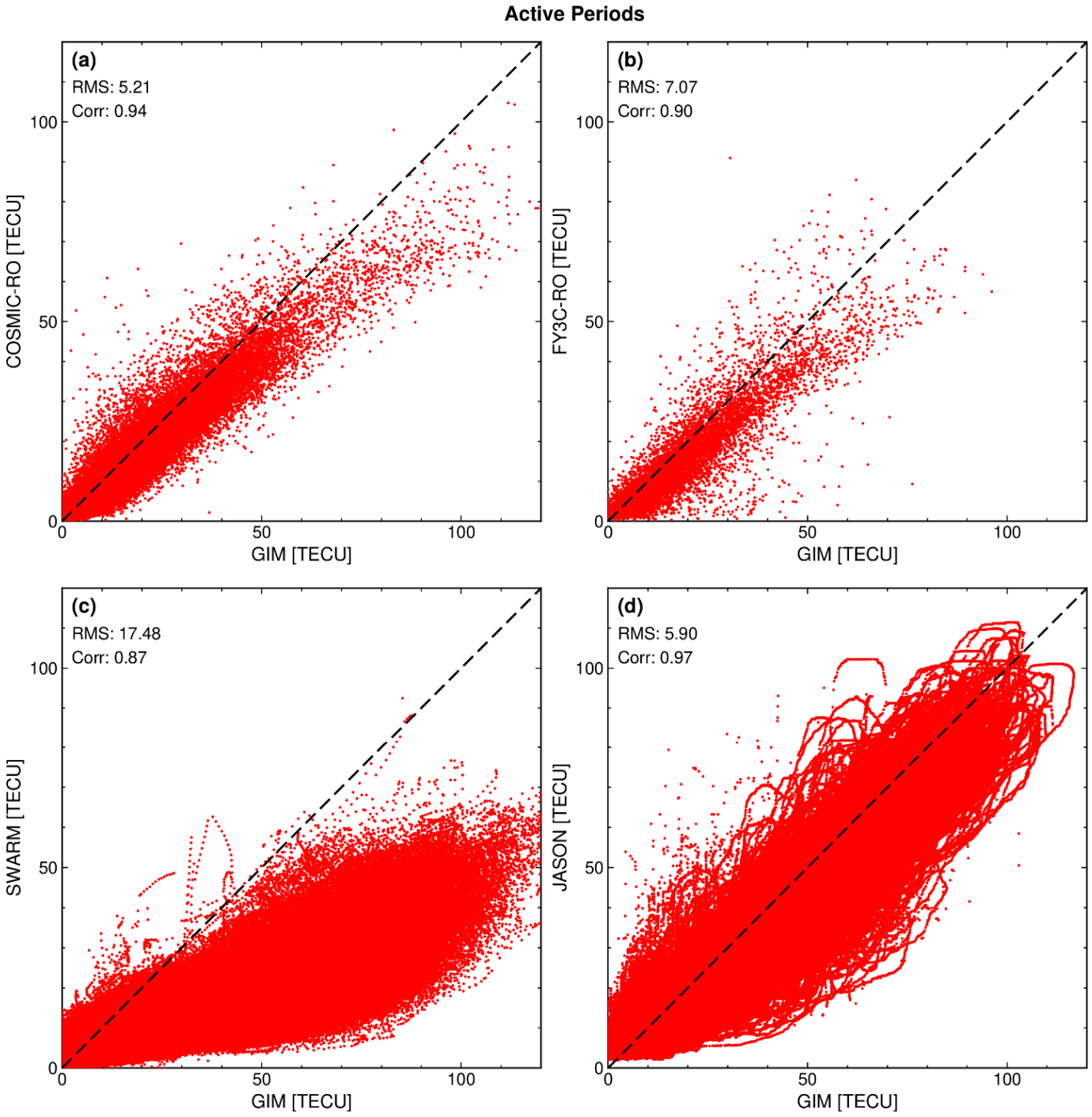


Figure 18. Scatter plots of VTEC values retrieved from COSMIC–RO (**a**), FY3C–RO (**b**), SWARM (**c**), and JASON (**d**) with GIM–VTEC for the active period.

6. Conclusions

In this study, VTEC values of different data sources for daily and long-term were analyzed on a global scale with a comparative approach.

Firstly, the quality of COSMIC RO, FY3C, SWARM, and JASON–VTEC was analyzed by using corresponding GIM–VTEC values for geomagnetic/solar active and quiet days. As a result of the daily VTEC comparisons, it was determined that the differences increased on active days. The differences obtained according to the GIM–VTEC values showed that the JASON–VTEC was closer to the GIM–VTEC. The most important reason for this is the coverage range of the JASON in the vertical direction. The RMSE values of JASON are

5.75 TECU, 5.20 TECU, and 4.93 TECU for geomagnetic active, solar active, and quiet days, respectively. Furthermore, the most significant difference was observed in SWARM.

Secondly, long-term results were examined using 123 active (solar and geomagnetic) and 242 quiet days in 2015. Results show that the RMSE of COSMIC RO, FY3C, SWARM, and JASON–VTEC are 5.02 TECU, 6.81 TECU, 16.25 TECU, and 5.53 TECU in the quiet period and 5.21 TECU, 7.07 TECU, 17.48 TECU, and 5.90 TECU in the active period, respectively. Similar to the daily comparison, the RMSE values of SWARM are larger and increase in the active period. Because the vertical coverage of SWARM is about 462/511 km to 20,200 km, it encompasses only a portion of the upper ionosphere. In order to further examine the consistency of the results, the correlation coefficients were calculated. The results indicate that JASON–VTEC has a better correlation with GIM–VTEC for both ionospheric conditions (97%).

The most important reason for these differences is the vertical coverage range of the data sources. While COSMIC RO provides VTEC data including the ionosphere and plasmasphere, FY3C RO does not include the upper ionosphere and plasmasphere; JASON 2–3 includes the ionospheric part, whereas SWARM A–C and B do not include the lower ionosphere as well as a significant part of the upper ionosphere with high electron density.

All these data sources have advantages and disadvantages compared to each other in terms of the data they provide. For instance, when considering the location of GNSS stations, GIM–VTEC data derived from observation data show superior quality for land areas in contrast to oceanic regions, while JASON provides high-quality VTEC data only for ocean regions. Although the COSMIC RO and FY3C RO results are expected to be similar, it appears that the COSMIC–RO data gives better results as it additionally provides data on the plasmaspheric part. However, due to the observation noise of the derived data from multi-instruments, gross errors should be removed using suitable methods. Considering all these aspects, it may be feasible to present global VTEC maps in an appropriate format using all data sources.

Author Contributions: Conceptualization, G.O. and S.A.; Methodology, G.O. and H.D.; data curation, H.D. and S.O.; visualization, G.O. and B.N.O.; writing—original draft preparation, G.O., S.A. and S.O. All authors have read and agreed to the published version of the manuscript.

Funding: This research received no external funding.

Institutional Review Board Statement: Not applicable.

Informed Consent Statement: Not applicable.

Data Availability Statement: The data presented in this study are available on request from the corresponding author. The data are not publicly available due to future publications.

Acknowledgments: We would like to thank the Center for Orbit Determination in Europe (CODE) for providing GIM data. We thank the NASA/GSFC's Space Physics Data Facility's OMNIWeb service "https://omniweb.gsfc.nasa.gov/ (accessed on 19 January 2024)". for Kp, Dst and F10.7 indices. We are grateful to the European Space Agency (ESA) of VirES service for providing the SWARM data "https://swarm-diss.eo.esa.int/#swarm (accessed on 15 January 2024)", to Open Altimeter Database (OpenADB) of the DGFI–TUM service for JASON data "https://openadb.dgfi.tum.de/en/ (accessed on 12 January 2024)", to University Corporation for Atmospheric Research (UCAR) COSMIC Data Analysis and Archive Center (CDAAC) for COSMIC data "https://cdaac-www.cosmic.ucar.edu/cdaac/products.html (accessed on 18 January 2024)", to National Satellite Meteorological Center of China "http://satellite.nsmc.org.cn (accessed on 20 January 2024)" FENGYUN Satellite Data Center for FY3C RO data.

Conflicts of Interest: The authors declare no conflicts of interest.

References

1. López-Urias, C.; Vazquez-Becerra, G.E.; Nayak, K.; López-Montes, R. Analysis of ionospheric disturbances during x-class solar flares (2021–2022) using GNSS data and wavelet analysis. *Remote Sens.* **2023**, *15*, 4626. [CrossRef]

2. Zhang, S.-R.; Nishimura, Y.; Erickson, P.J.; Aa, E.; Kil, H.; Deng, Y.; Thomas, E.G.; Rideout, W.; Coster, A.J.; Kerr, R.; et al. Traveling ionospheric disturbances in the vicinity of storm-enhanced density at midlatitudes. *J. Geophys. Res. Space Phys.* **2022**, *127*, e2022JA030429. [CrossRef] [PubMed]
3. Essien, P.; Figueiredo, C.A.O.B.; Takahashi, H.; Wrasse, C.M.; Barros, D.; Klutse, N.A.B.; Lomotey, S.O.; Ayorinde, T.T.; Gobbi, D.; Bilibio, A.V. Long-Term study on medium-scale traveling ionospheric disturbances observed over the South American Equatorial Region. *Atmosphere* **2021**, *12*, 1409. [CrossRef]
4. Atabati, A.; Alizadeh, M.; Schuh, H.; Tsai, L.-C. Ionospheric scintillation prediction on S4 and ROTI parameters using artificial neural network and genetic algorithm. *Remote Sens.* **2021**, *13*, 2092. [CrossRef]
5. Feng, J.; Yuan, Y.; Zhang, T.; Zhang, Z.; Meng, D. Analysis of ionospheric anomalies before the Tonga volcanic eruption on 15 January 2022. *Remote Sens.* **2023**, *15*, 4879. [CrossRef]
6. Nayak, K.; López-Urías, C.; Romero-Andrade, R.; Sharma, G.; Guzmán-Acevedo, G.M.; Trejo-Soto, M.E. Ionospheric Total Electron Content (TEC) anomalies as earthquake precursors: Unveiling the geophysical connection leading to the 2023 Moroccan 6.8 Mw Earthquake. *Geosciences* **2023**, *13*, 319. [CrossRef]
7. Bilitza, D. International Reference Ionosphere 2000. *Radio Sci.* **2001**, *36*, 261–275. [CrossRef]
8. Daniell, R.E., Jr.; Brown, L.D.; Anderson, D.N.; Fox, M.W.; Doherty, P.H.; Decker, D.T.; Sojka, J.J.; Schunk, R.W. Parameterized ionospheric model: A global ionospheric parameterization based on first principles models. *Radio Sci.* **1995**, *30*, 1499–1510. [CrossRef]
9. Bent, R.B.; Llewellyn, S.K. *Documentation and Description of the Bent Ionospheric Model*; Space and Missile Organisation: Los Angeles, CA, USA, 1973.
10. Hochegger, G.; Nava, B.; Radicella, S.M.; Leitinger, R. A family of ionospheric models for different uses. *Phys. Chem. Earth Part C Sol. Terr. Planet. Sci.* **2000**, *25*, 307–310. [CrossRef]
11. Radicella, S.M.; Leitinger, R. The evolution of the DGR approach to model electron density profiles. *Adv. Space Res.* **2001**, *27*, 35–40. [CrossRef]
12. Anderson, D.N.; Mendillo, M.; Herniter, B. A semi-empirical low latitude ionospheric model. *Radio Sci.* **1987**, *22*, 292–306. [CrossRef]
13. Gulyaeva, T.L.; Huang, X.; Reinisch, B.W. Plasmaspheric extension of topside electron density profiles. *Adv. Space Res.* **2002**, *29*, 825–831. [CrossRef]
14. Alcay, S. Analysis of the TEC prediction performance of IRI-2016 model in the mid-latitude region. *Geomagn. Aeron.* **2021**, *61*, 600–618. [CrossRef]
15. Bilitza, D.; Pezzopane, M.; Truhlik, V.; Altadill, D.; Reinisch, B.W.; Pignalberi, A. The International Reference Ionosphere model: A review and description of an ionospheric benchmark. *Rev. Geophys.* **2022**, *60*, e2022RG000792. [CrossRef]
16. Jakowski, N.; Heise, S.; Stankov, S.M.; Tsybulya, K. Remote sensing of the ionosphere by space-based GNSS observations. *Adv. Space Res.* **2006**, *38*, 2337–2343. [CrossRef]
17. Shah, M.; Shahzad, R.; Jamjareegulgarn, P.; Ghaffar, B.; Oliveira-Júnior, J.F.d.; Hassan, A.M.; Ghamry, N.A. Machine-Learning -Based Lithosphere-Atmosphere- Ionosphere Coupling Associated with Mw > 6 Earthquakes in America. *Atmosphere* **2023**, *14*, 1236. [CrossRef]
18. Nayak, K.; Romero-Andrade, R.; Sharma, G.; Zavala, J.L.C.; Urias, C.L.; Trejo Soto, M.E.; Aggarwal, S.P. A combined approach using b-value and ionospheric GPS-TEC for large earthquake precursor detection: A case study for the Colima earthquake of 7.7 Mw, Mexico. *Acta Geod. Geophys.* **2023**, *58*, 515–538. [CrossRef]
19. Sharma, G.; Nayak, K.; Romero-Andrade, R.; Aslam, M.M.; Sarma, K.K.; Aggarwal, S.P. low ionosphere density above the earthquake epicentre region of Mw 7.2, El Mayor–Cucapah earthquake evident from dense CORS data. *J. Indian Soc. Remote Sens.* **2024**, *52*, 543–555. [CrossRef]
20. Milanowska, B.; Wielgosz, P.; Krypiak-Gregorczyk, A.; Jarmołowski, W. Accuracy of Global Ionosphere Maps in relation to their time interval. *Remote Sens.* **2021**, *13*, 3552. [CrossRef]
21. Senturk, E.; Çepni, M.S. Performance of different weighting and surface fitting techniques on station-wise TEC calculation and modified sine weighting supported by the sun effect. *J. Spat. Sci.* **2019**, *64*, 209–220. [CrossRef]
22. Schaer, S.; Gurtner, W.; Feltens, J. IONEX: The ionosphere map exchange format version 1. In Proceedings of the IGS AC Workshop, Darmstadt, Germany, 25 February 1998; Volume 9, pp. 1–15.
23. Astafyeva, E.; Zakharenkova, I.; Förster, M. Ionospheric response to the 2015 St. Patrick's Day storm: A global multi-instrumental overview. *J. Geophys. Res. Space Phys.* **2015**, *120*, 9023–9037. [CrossRef]
24. Lin, C.Y.; Lin, C.C.H.; Liu, J.Y.; Rajesh, P.K.; Matsuo, T.; Chou, M.Y.; Tasi, H.F.; Yeh, W.H. The early results and validation of FORMOSAT-7/COSMIC-2 space weather products: Global ionospheric specification and Ne-aided Abel electron density profile. *J. Geophys. Res. Space Phys.* **2020**, *125*, e2020JA028028. [CrossRef]
25. Spogli, L.; Sabbagh, D.; Regi, M.; Cesaroni, C.; Perrone, L.; Alfonsi, L.; Di Mauro, D.; Lepidi, S.; Campuzano, S.A.; Marchetti, D.; et al. Ionospheric response over Brazil to the August 2018 geomagnetic storm as probed by CSES-01 and Swarm satellites and by local ground based observations. *J. Geophys. Res. Space Phys.* **2021**, *126*, e2020JA028368. [CrossRef]
26. Vardhan, A.; Babu Sree Harsha, P.; Venkata Ratnam, D.; Upadhayaya, A.K. Low latitude ionospheric response to March 2015 geomagnetic storm using multi-instrument TEC observations over India. *Astrophys. Space Sci.* **2020**, *365*, 187. [CrossRef]

27. Xu, J.; Wang, Q.; Ke, F.; Zhang, B.; Yan, C.; Zhang, H. Analysis of ionospheric parameters retrieved from Feng-Yun 3C and COSMIC radio occultation. *Adv. Space Res.* **2021**, *68*, 214–224. [CrossRef]
28. Azpilicueta, F.; Nava, B. On the TEC bias of altimeter satellites. *J. Geod.* **2021**, *95*, 114. [CrossRef]
29. Zhang, R.; Le, H.; Li, W.; Ma, H.; Yang, Y.; Huang, H.; Li, Q.; Zhao, X.; Xie, H.; Sun, W.; et al. Multiple technique observations of the ionospheric responses to the 21 June 2020 solar eclipse. *J. Geophys. Res. Space Phys.* **2021**, *125*, e2020JA028450. [CrossRef]
30. Atabati, A.; Jazireeyan, I.; Alizadeh, M.; Pirooznia, M.; Flury, J.; Schuh, H.; Soja, B. Analyzing the Ionospheric Irregularities Caused by the September 2017 Geomagnetic Storm Using Ground-Based GNSS, Swarm, and FORMOSAT-3/COSMIC Data near the Equatorial Ionization Anomaly in East Africa. *Remote Sens.* **2023**, *15*, 5762. [CrossRef]
31. Emmela, S.; Ratnam, D.V.; Leong, T.E. Regional ionospheric TEC modeling during geomagnetic storm in August 2021-data fusion using multi-instrument observations. *Adv. Space Res.* **2024**, *73*, 3818–3832. [CrossRef]
32. Jiang, C.; An, Q.; Wang, S.; Nie, W.; Zhu, H.; Liu, G. Accuracy assessment of the ionospheric total electron content derived from COSMIC-2 radio occultation based on multi-source data. *Adv. Space Res.* **2024**, *73*, 5157–5170. [CrossRef]
33. Yang, H.; Monte-Moreno, E.; Hernández-Pajares, M.; Roma-Dollase, D. Real-time interpolation of global ionospheric maps by means of sparse representation. *J. Geod.* **2021**, *95*, 71. [CrossRef]
34. Available online: https://cdaac-www.cosmic.ucar.edu/ (accessed on 18 January 2024).
35. Bai, W.; Tan, G.; Sun, Y.; Xia, J.; Cheng, C.; Du, Q.; Wang, X.; Yang, G.; Liao, M.; Liu, Y.; et al. Comparison and validation of the ionospheric climatological morphology of FY3C/GNOS with COSMIC during the recent low solar activity period. *Remote Sens.* **2019**, *11*, 2686. [CrossRef]
36. Zhao, Q.; Wang, C.; Guo, J.; Yang, G.; Liao, M.; Ma, H.; Liu, J. Enhanced orbit determination for BeiDou satellites with FengYun-3C onboard GNSS data. *GPS Solut.* **2017**, *21*, 1179–1190. [CrossRef]
37. Available online: http://satellite.nsmc.org.cn (accessed on 20 January 2024).
38. Piersanti, M.; Pezzopane, M.; Zhima, Z.; Diego, P.; Xiong, C.; Tozzi, R.; Pignalberi, A.; D'Angelo, G.; Battiston, R.; Huang, J.; et al. Can an impulsive variation of the solar wind plasma pressure trigger a plasma bubble? A case study based on CSES, Swarm, and THEMIS data. *Adv. Space Res.* **2021**, *67*, 35–45. [CrossRef]
39. Satti, M.S.; Ehsan, M.; Abbas, A.; Shah, M.; Oliveira-Júnior, J.F.D.; Naqvi, N. A Atmospheric and ionospheric precursors associated with Mw≥6.5 earthquakes from multiple satellites. *J. Atmos. Sol. Terr. Phys.* **2022**, *227*, 105802. [CrossRef]
40. VirES. Available online: https://vires.services/ (accessed on 15 January 2024).
41. Available online: https://swarmhandbook.earth.esa.int/article/documentation (accessed on 15 January 2024).
42. Available online: https://www.ncei.noaa.gov/sites/default/files/2021-01/Jason-3%20Products%20Handbook.pdf (accessed on 15 January 2024).
43. Available online: https://www.ncei.noaa.gov/data/oceans/ (accessed on 17 January 2024).
44. Alcay, S.; Gungor, M. Investigation of ionospheric TEC anomalies caused by space weather conditions. *Astrophys. Space Sci.* **2020**, *365*, 150. [CrossRef]
45. Available online: https://omniweb.gsfc.nasa.gov/form/dx1.html (accessed on 19 January 2024).

Disclaimer/Publisher's Note: The statements, opinions and data contained in all publications are solely those of the individual author(s) and contributor(s) and not of MDPI and/or the editor(s). MDPI and/or the editor(s) disclaim responsibility for any injury to people or property resulting from any ideas, methods, instructions or products referred to in the content.